Feasibility study of the use of similarity maps in the evaluation of oncological dynamic positron emission tomography images

T. Thireou[1]   G. Kontaxakis[2]   L. G. Strauss[3]
A. Dimitrakopoulou-Strauss[3]   S. Pavlopoulos[1]   A. Santos[2]

[1]Biomedical Engineering Laboratory, National Technical University of Athens, Athens, Greece
[2]ETSI de Telecomunicacion, Universidad Politecnica de Madrid, Madrid, Spain
[3]Medical PET Group, Biological Imaging, German Cancer Research Center, Heidelberg, Germany

Abstract—*A preliminary study is presented on the potential role of similarity mapping (SM) in the evaluation of oncological dynamic ^{18}F-fluorodeoxyglucose positron emission tomography studies, mainly in lesion localisation and detectability. Similarity maps were calculated using previously described (correlation coefficient (COR) and normalised correlation coefficient (NCOR)) and newly introduced similarity measures (sum of squares coefficient (SSQ), squared sum coefficient (SQS), sum of cubes coefficient (SC) and cubed sum coefficient (CS)). The results were evaluated using simulated and clinical data. The study revealed that the best-suited similarity measure for such applications was the CS similarity coefficient, which provided the best parametric images, delineating structures of interest and supporting the visual interpretation of data sets. It was shown that SM and standardised uptake value (SUV) images had comparable diagnostic performance, although SM was able to offer additional time-related information in a single image. For the case of colorectal recurrences (17 cases), the measured contrast values for the CS and SUV images were 2.36 ± 0.47 and 4.12 ± 0.42, respectively, whereas, for three cases of giant cell tumours, these values were 11.6 ± 2.1 and 11.9 ± 1.8, respectively.*

Keywords—*Similarity mapping, Positron emission tomography, Feature extraction, Dynamic PET, Standardized uptake value*

1 Introduction

POSITRON EMISSION tomography (PET) provides physicians with unique diagnostic information that can improve patient management and reduce the total cost of patient care (GAMBHIR *et al.*, 2001; PHELPS, 2004). It produces images of molecular-level physiological function that can be used to measure many vital processes, such as glucose metabolism, blood flow and oxygen utilisation.

PET allows the assessment of chemical and physiological changes related to metabolism. This is important because functional change often predates structural changes in tissues. PET images can therefore demonstrate pathological changes long before they would be revealed by modalities such as computerised tomography (CT) and magnetic resonance imaging (MRI).

Unlike traditional nuclear medicine, PET uses unique radio-pharmaceuticals that are the basic elements of biological

substrates. These tracers mimic natural substrates such as sugars, water, proteins and oxygen. As a result, PET will often reveal more about the cellular-level metabolic status of a disease than other types of imaging modality.

After extensive investigation in experimental and clinical oncology, ^{18}F-fluorodeoxyglucose (^{18}F-FDG) PET has been proved to be a valuable imaging technique for the evaluation of a variety of tumours (ALAVI and REIVICH, 2002; JERUSALEM *et al.*, 2003). Visual inspection of PET images is the practice routinely used for tumour diagnosis and evaluation. However, quantitative measures based on the normalisation of tracer concentrations for the injected activity and body weight (standardised uptake values, (SUVs)) are becoming common in clinical practice of oncological PET (STRAUSS and CONTI, 1991).

The SUV approach, however, represents a static measurement of the tracer accumulation within the time of the data acquisition and does not take into account the fact that ^{18}F-FDG uptake is a dynamic process. Dynamic ^{18}F-FDG PET studies (temporal sequences of images in the same bed position) offer differential diagnostic information and therefore are the most accurate approach to quantify ^{18}F-FDG kinetics. Such studies are being increasingly used in oncological PET

studies for diagnosis, therapy management and evaluation (STRAUSS *et al.*, 2003).

To increase the accuracy of localising primary tumours and metastases and to improve the prognosis of patients, several methods have been proposed for the analysis of dynamic studies, including compartmental and non-compartmental approaches (STRAUSS *et al.*, 1998), principal component analysis (THIREOU *et al.*, 2003) and non-negative matrix factorisation (LEE *et al.*, 2001). In this context, we have investigated the performance of similarity maps (SMs).

Similarity mapping involves the definition of a reference region of interest (RROI) and the correlation of the pixel value intensity time distribution (or time activity curve, (TAC)) with this reference curve to form a similarity map (temporal match). The analysis is performed using pixel-by-pixel analysis of the dynamic image series. The generated result of this analysis is a similarity map where the value of each pixel measures its temporal similarity to the reference. In this way, the whole image sequence is reduced to a single image (similarity map), where each pixel value is set equal to the value of the similarity parameter at that point. This approach can be also considered as a segmentation tool, segmenting an image into regions with the same temporal properties (AMARAL *et al.*, 1998).

Using similarity measurement techniques, background noise or contrast signal originating from the superposition of structures without clinical interest or significance can be efficiently removed. This signal de-noising property, however, does not imply that noise related to the physics of positron annihilation (e.g. positron range) and g-ray detection (e.g. partial volume effects, non-accurate scatter and attenuation corrections) can also be corrected with this method.

Similarity maps segment multidimensional images into regions according to their temporal rather than spatial properties (ROGOWSKA *et al.*, 1994). SM images therefore provide spatially differentiated quantitative information describing the physiological behaviour of the image structures, which sometimes cannot easily be extracted from visual inspection of dynamic PET image sequences. Several measures can describe the similarity, including the cross-correlation coefficient (ROGOWSKA *et al.*, 1995), the sum of absolute valued difference (SAVD) (BARNEA and SILVERMAN, 1972), the stochastic sign change (SSC) criterion (VENOT *et al.*, 1984) and the Tanimoto coefficient (TANIMOTO, 1961), a similarity coefficient commonly used in chemical informatics.

Similarity mapping has been applied to CT images of rabbits with focal cerebral ischaemia and was able to identify small differences in the temporal dynamics around the infarct (LO *et al.*, 1996). SM has also been applied in time series of cardiac images in regions of similar temporal behaviour to capture the essential information of the sequence while reducing the number of image data presented to the clinician for diagnostic interpretation (BOUDRAA *et al.*, 1999). Other applications include the use of similarity transformations to match two images with different resolutions (DUFOURNAUD *et al.*, 2004).

Spectral SM segments images according to their spectral characteristics and has been used in combination with spectral imaging and electron microscopy to extract differentiation parameters for several types of cell (ROTHMANN *et al.*, 2000; HYMAN *et al.*, 2001). An example of the numerous applications of SM in fields other than imaging is its use in spoken word recognition, where most models assume lexical representations are activated based on the degree of similarity of the acoustic-phonetic input to a stored lexical representation (CONNINE *et al.*, 1997).

In this work, we present the application of similarity maps to the identification of clinically significant features in simulated dynamic PET image sets. To demonstrate the feasibility of the application of the proposed methods to such kinds of image sequence, clinical data sets from oncological PET studies were used, and the results of this preliminary evaluation study are given.

2 Materials and methods

2.1 Similarity mapping

Two of the similarity measures previously described (ROGOWSKA *et al.*, 1994; 1995) were used for the calculation of similarity maps: the correlation coefficient *COR* and normalised correlation coefficient *NCOR*.

$$COR_{ij} = \frac{\sum_{n=1}^{N} A_{ijn} R_n}{\sqrt{\sum_{n=1}^{N} A_{ijn}^2 \sum_{n=1}^{N} R_n^2}} \tag{1}$$

$$NCOR_{ij} = \frac{\sum_{n=1}^{N} (A_{ijn} - \mu_{Aij})(R_n - \mu_R)}{\sqrt{\sum_{n=1}^{N} (A_{ijn} - \mu_{Aij})^2 \sum_{n=1}^{N} (R_n - \mu_R)^2}} \tag{2}$$

where N is the number of frames, A_{ijn} is the value of pixel (i, j) in frame n; R_n is the value of the TAC of the RROI; μ_R is the mean value of the reference TAC; and μ_{Aij} is the mean value of pixel (i, j) TAC.

The result from the application of each of the above algorithms to a sequence of frames from a dynamic PET study is one image per tomographic slice, where each pixel value represents the degree of temporal similarity of area A to reference region R. Both correlation and normalised correlation maps have values ranging from -1 (for regions that are perfect 'negatives' of the reference ROI's TAC: TAC_{ref}) to $+1$ (for regions that are identical to TAC_{ref}). Although both measures are normalised for proportional differences ($TAC = a \times TAC_{ref}$, $a = $ const), only the NCOR is normalised for additive differences ($TAC = a + TAC_{ref}$, $a = $ const) (ROGOWSKA *et al.*, 1994).

Although COR and NCOR were able to identify several structures in dynamic MRI images (ROGOWSKA *et al.*, 1994; 1995; BANDETTINI *et al.*, 1993; LUCAS-QUESADA *et al.*, 1996; BOUDRAA *et al.*, 2001), they proved to be ineffective in analysing dynamic PET studies (see Section 3). As new similarity measures were required, we introduced the following formulas: sum of squares coefficient *SSQ*, squared sum coefficient *SQS*, sum of cubes coefficient *SC* and cubed sum coefficient *CS*:

$$SSQ_{ij} = \frac{\sum_{n=1}^{N} (A_{ijn} - \mu_{Aij})^2 (R_n - \mu_R)^2}{\mu_R \sqrt{\sum_{n=1}^{N} (A_{ijn} - \mu_{Aij})^2 \sum_{n=1}^{N} (R_n - \mu_R)^2}} \tag{3}$$

$$SQS_{ij} = \frac{\left(\sum_{n=1}^{N} (A_{ijn} - \mu_{Aij})(R_n - \mu_R)\right)^2}{\mu_R \sqrt{\sum_{n=1}^{N} (A_{ijn} - \mu_{Aij})^2 \sum_{n=1}^{N} (R_n - \mu_R)^2}} \tag{4}$$

$$SC_{ij} = \frac{\sum_{n=1}^{N} (A_{ijn} - \mu_{Aij})^3 (R_n - \mu_R)^3}{\mu_R^2 \sqrt{\sum_{n=1}^{N} (A_{ijn} - \mu_{Aij})^2 \sum_{n=1}^{N} (R_n - \mu_R)^2}} \tag{5}$$

$$CS_{ij} = \frac{\left(\sum_{n=1}^{N} (A_{ijn} - \mu_{Aij})(R_n - \mu_R)\right)^3}{\mu_R^2 \sqrt{\sum_{n=1}^{N} (A_{ijn} - \mu_{Aij})^2 \sum_{n=1}^{N} (R_n - \mu_R)^2}} \tag{6}$$

SSQ and SQS provide a similarity measure normalised for additive differences and perfect negatives and have values ranging from 0 (for totally uncorrelated regions) to a maximum value different in each case. SC and CS are normalised for additive differences and range from negative values (for regions with opposite TACs) to positive values.

Values in the similarity map images also depend on the intensity levels at the RROI's TAC and the TACs of the rest of the pixel values. Therefore, even in the case of similar temporal behaviour for the RROI and another ROI in one image sequence, the similarity map values will also reflect the proportional difference between those two regions.

In the case of PET image sequences, proper decay corrections should be performed before SM methods are applied. Another important parameter that could lead to erroneous results is lack of spatial registration between image frames for the same tomographic slice. To classify voxels or volumes/regions of interest correctly, based on similarity criteria, the images should previously be checked for spatial registration. Patient motion and respiratory artifacts should therefore be corrected prior to the application of SM. To compensate for such possible errors, for this study, the original ROIs were visually repositioned but not redrawn. At present, there is no technique available for the clinical routine that would correct for patient motion or respiratory artifacts, although such methods are currently being investigated. An evaluation of the robustness of the method as a function of motion is, however, outside the scope of this study.

Where similarity maps are to be applied to sequences of images taken at different times (e.g. before, during and after treatment) to evaluate the tumour response to therapy, then spatial registration, as well as appropriate selection of the anatomically identical slices from each image volume, should be carefully applied before the application of SM methods.

2.2 Dynamic phantom

To evaluate the performance of the similarity measures developed before their application to real clinical cases, a dynamic data set was created simulating an image series from a lower abdomen PET study. For this purpose, a one-slice phantom image was created. This phantom image is shown in Fig. 1 and consists of a big ellipse M corresponding to normal tissue masses (which, for real PET scans, could include, apart from muscle, gut, fat, fine vasculature, other soft tissue structures and bones of the pelvis), and three smaller ellipses corresponding to the bladder B, tumour T and vessel V.

The time activity curves were generated based on the TACs measured in a real dynamic ^{18}F-FDG PET study from a case of colorectal tumour recurrence, including the noise characteristics of the measured data. This guaranteed that the simulation results were performed at realistic noise levels. The study consisted of 23 frames (30 s, 9 × 60 s, 90 s, 4 × 120 s, 210 s, 7 × 300 s). From this study, appropriate ROIs were placed over areas corresponding to normal tissue, tumour, bladder and vessels, and the TACs were calculated for each of these regions. The results are also shown in Fig. 1.

2.3 Clinical data

The study included 17 patients with colorectal tumour recurrences and three patients with giant cell tumour, who were referred on the basis of clinical symptoms and radiological
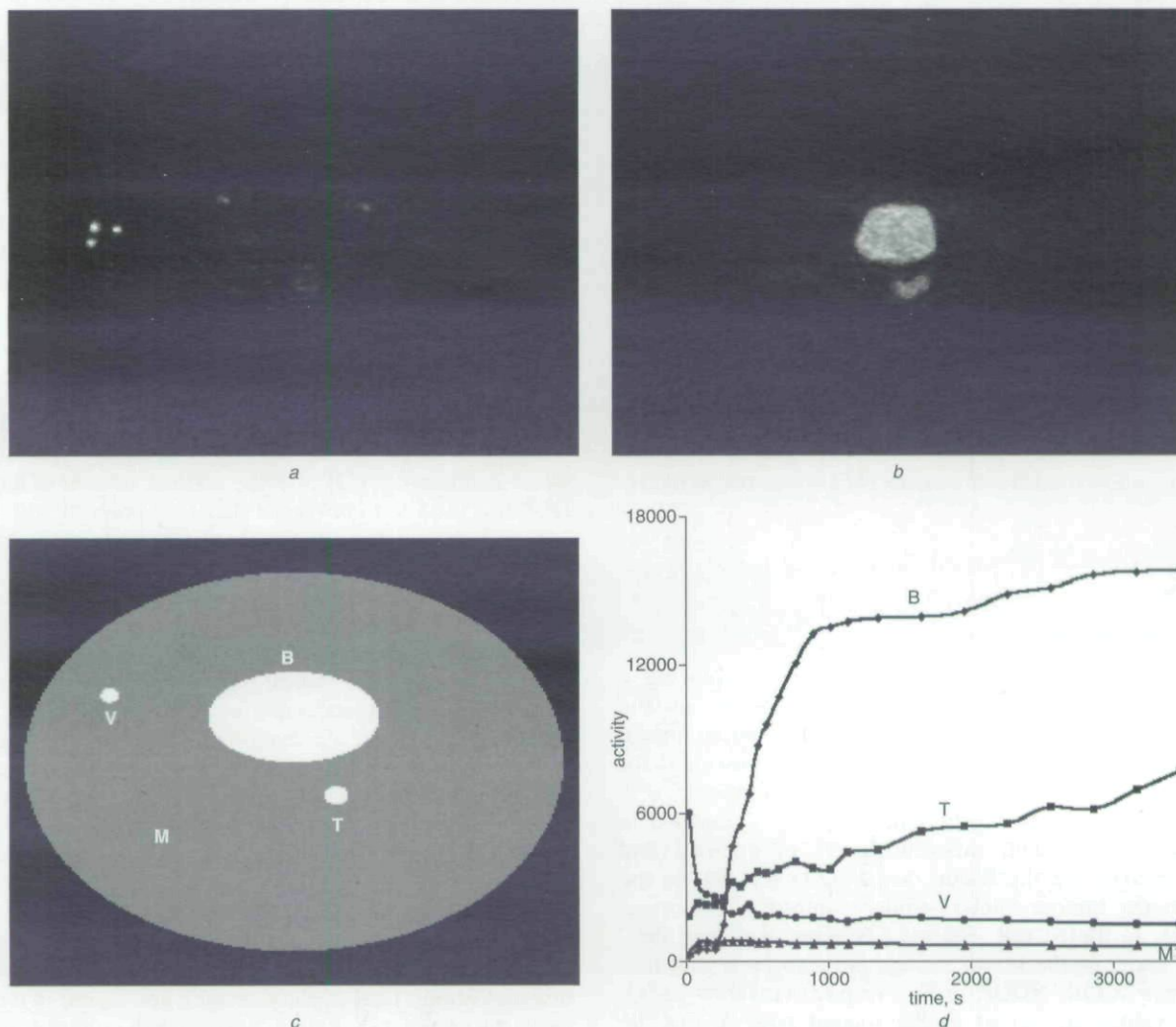
Fig. 1   (a) First and (b) last frame of real patient dynamic PET study used for formation of (c) simulated dynamic PET phantom image series. (d) Time activity curves from study were used as basis for definition of corresponding TAC functions of phantom

examinations, either CT or MRI. The final diagnosis was based on the histological data obtained from surgical specimens. None of the patients had received chemotherapy or radiation therapy at least 3 months prior to the PET study. Informed consent was obtained from each patient. The study was performed in accordance with the institutional review board requirements.

Dynamic PET studies were performed after intravenous injection of 300–370 MBq ^{18}F-FDG for 60 min. A 23-frame protocol was used (10 × 1 min, 5 × 2 min and 8 × 5 min). ^{18}F-FDG was prepared according to the protocol described by TOORONGIAN (1990).

A dedicated PET system* was used for the patient studies (BRIX et al., 1997; ADAM et al., 1997). The system consists of four rings of 72 BGO detector blocks. Each block detector is divided into an 8×8 matrix, and the crystal size of an individual detector element is 4.39 × 4.05 × 30 mm. The system allows the simultaneous acquisition of 63 transverse slices, with a theoretic slice thickness of 2.4 mm, and has an axial field of view of 15.3 cm. The system was operated in two-dimensional mode (with septa extended). Transmission scans were obtained for a total of 10 min with three rotating germanium pin sources, before the first radionuclide application for the attenuation correction of the acquired emission tomographic images.

All PET images were attenuation corrected. An image matrix of 128 × 128 pixels was used. The images were reconstructed using an iterative reconstruction algorithm (weighted least-square method, ordered subsets, four subsets, six iterations) (KONTAXAKIS et al., 2002), and the standardised uptake values (SUVs) were calculated (STRAUSS and CONTI, 1991)

$$SUV = \frac{tissue\ concentration\ (MBq\,g^{-1})}{(injected\ activity\ (MBq)/body\ weight\ (g))}$$

The SUV calculations were performed based on the last study frame (55–60 min post injection). No partial volume correction was performed; however, SUV measurements were performed on volumes of interest (VOIs) spanning several tomographic slices, instead of the conventional methods that average the measured concentration over an ROI drawn in just one slice.

The similarity map images were evaluated mainly by calculating the contrast of the tumour area with normal tissue. Contrast is measured as $CR = (T - M)/M$, where T and M are the mean activities of pixels in ROIs placed over the tumour (T) and normal tissue masses (M) areas, respectively.

3 Results

3.1 Dynamic phantom

We first applied the similarity coefficients by placing a reference ROI over the bladder ROI_b and another on the normal tissue mass ROI_m of the simulated phantom image series. Table 1 summarises the contrast values measured for each of the similarity coefficients for these two cases.

In the first case ROI_b, the tumour can be distinguished in all similarity maps with different levels of contrast and clarity. The SUV for the lesion (see Fig. 1) was 34. In the COR map, the tumour shows similar contrast with normal tissue areas. In the NCOR, SC and CS maps, it is well delineated. In some of the maps, vessels are also present, either with negative (COR, NCOR or SC) or positive values (SSQ, where all values are raised to the second power). For the case of the reference ROI_m in most of the maps, the tumour

Table 1 Contrast values for ROI$_b$ and ROI$_m$ for simulated phantom image series

ROI	COR	NCOR	SSQ	SQS	SC	CS
ROI_b	0.15	2.46	40.0	30.0	0.97	54.0
ROI_m	0.10	0.83	0.0	0.12	0.15	0.22

is visible, but has similar (low) contrast levels to the reference normal tissues. In NCOR it is well delineated, whereas, in SSQ, it cannot be detected.

For comparison, similarity maps were also calculated for the original dynamic PET study (shown in Fig. 1), using the same TACs and placing ROIs over the bladder (ROI_b, Fig. 2) and normal tissue masses (ROI_m, Fig. 3). For ROI_b, both the COR and NCOR maps are very noisy, and the tumour, located below the bladder, is 'guessed at' rather than clearly detected. In SSQ and SQS, the tumour is visible below a very bright bladder, whereas, in SC, it has similar intensity values to normal tissue and is not visible. In contrast, the CS map can clearly separate bladder and tumour from the other structures. For ROI_m, the tumour is slightly visible in NCOR, but no other similarity measure is able to detect it, as can be seen in the calculated contrast values, presented in Table 2, which summarises the contrast values measured for each of the similarity coefficients for these two cases.

As COR and NCOR values range over [−1, +1], normalisation of values for display results in amplification of small differences and therefore produces noisy images. In contrast, the other SM value intervals are larger, resulting in maps where only major differences are represented and that therefore can produce clearly separated structures.

In the presence of the high-activity bladder and the quickly disappearing vessel activity, in most of the maps, tumour similarity values are comparable with the normal tissue ones, and therefore the tumour cannot easily be detected. However, using the newly introduced CS measure and an ROI placed over the bladder, the resulting parametric image is comparable with the last frame SUV image, and the tumour is clearly revealed.

3.2 Clinical data

The time required for the analysis of a complete data set (23 frames, 32 slices per frame, 128 × 128 pixels per slice) was 40 s.† A reference VOI over the tumour, instead of a reference ROI, was used, to improve the statistical properties of the TAC.

Fig. 4 shows an example of six similarity maps calculated according to (1)–(6) for the same transaxial image slice of one data set from a clinical patient study (colorectal recurrence tumour). The contrast values calculated for this case are given in Table 3.

In SSQ and SQS similarity maps, both the tumour and the vessels are present, although, in SQS, the tumour is the predominant structure. As both measures are normalised for 'negative' differences, regions with almost opposite time activity curves, such as the tumour and the vessels, have similar values and are visible in the resulting map. However, the SQS enhances the differences and provides better results in revealing the structures of interest, without, however, providing information on the physiological differences of each region (vessel as against tumour).

In SC and CS similarity maps, tumours have positive values, whereas vessels have negative values, and therefore they can be easily discriminated (light as against dark colours). Moreover,
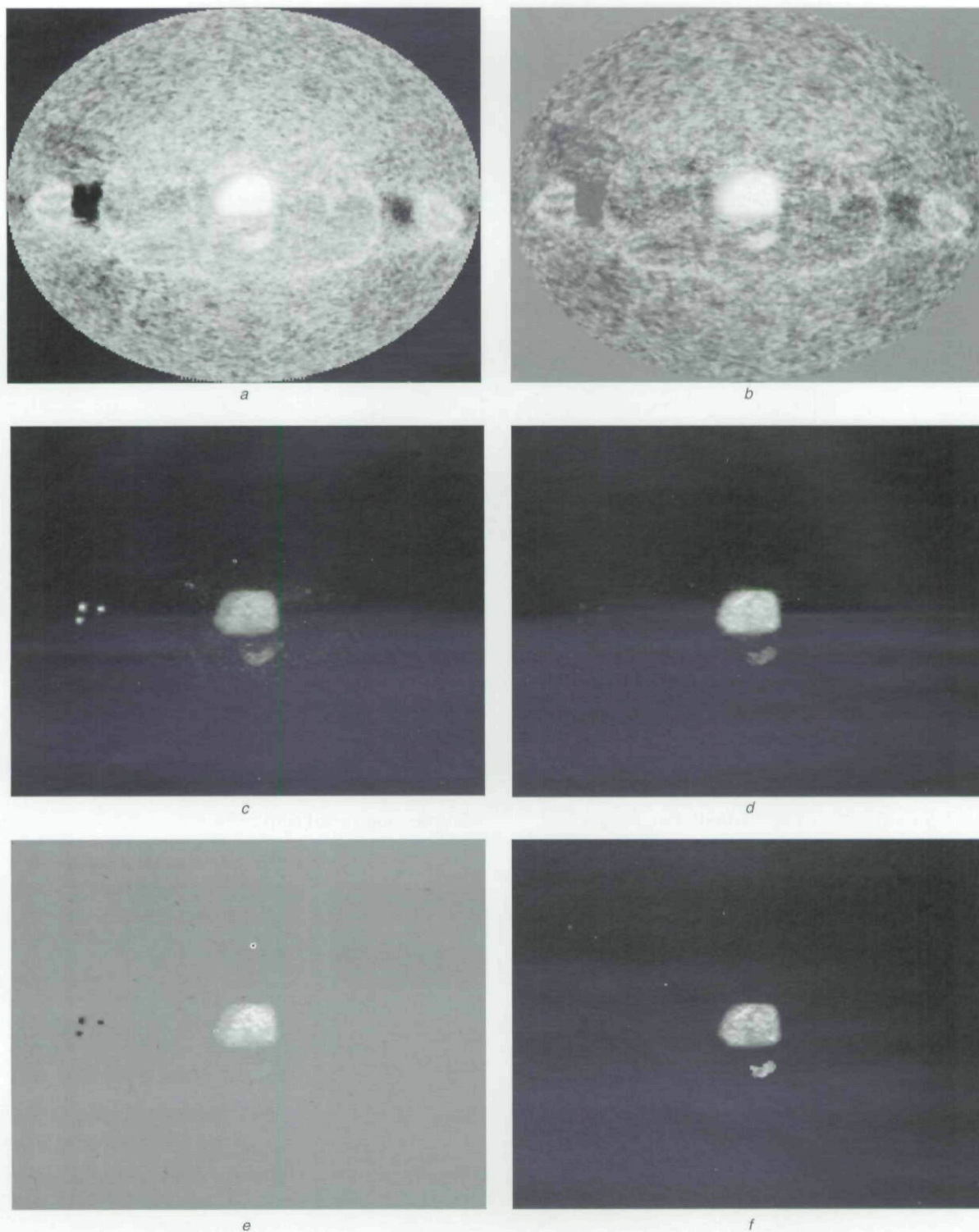
Fig. 2 *Similarity maps of dynamic PET study shown in Fig. 1, calculated using reference ROI placed over bladder and similarity measures (a) COR, (b) NCOR, (c) SSQ, (d) SQS, (e) SC and (f) CS*

in CS, the values of regions with quite different TACs (tumour against normal tissue) show greater variation than in SC, resulting in better contrast for the tumour areas. The ratio of mean intensities ROI_t/ROI_m for CS is twice that for SC, thus supporting the previous observation, where ROI_t represents a region of interest placed over the tumour area in the image.

Table 4 summarises the diagnostic performance (visual detection of tumours and vessels) of the similarity coefficients in all 20 patient studies. Similarity maps based on the correlation coefficient and the normalised correlation coefficient are very noisy, and the tumours cannot be separated from the other structures.

Fig. 5 shows a comparison of SM images (CS, upper row) with SUV images of the same studies (lower row). Fig. 5a shows a transaxial slice from a dynamic PET study of a patient with a giant cell tumour of the right tibia, and Figs 5b and c show two transaxial slices from dynamic ^{18}F-FGD PET studies of two patients with recurrent colorectal tumour. The similarity maps demonstrate lesions with enhanced FDG uptake, negatively delineate vessels and have comparable contrast with the SUV images. Table 5 shows the measured contrast values for the CS and SUV images for the 17 cases of colorectal cancer recurrence and the three cases of giant cell tumour.
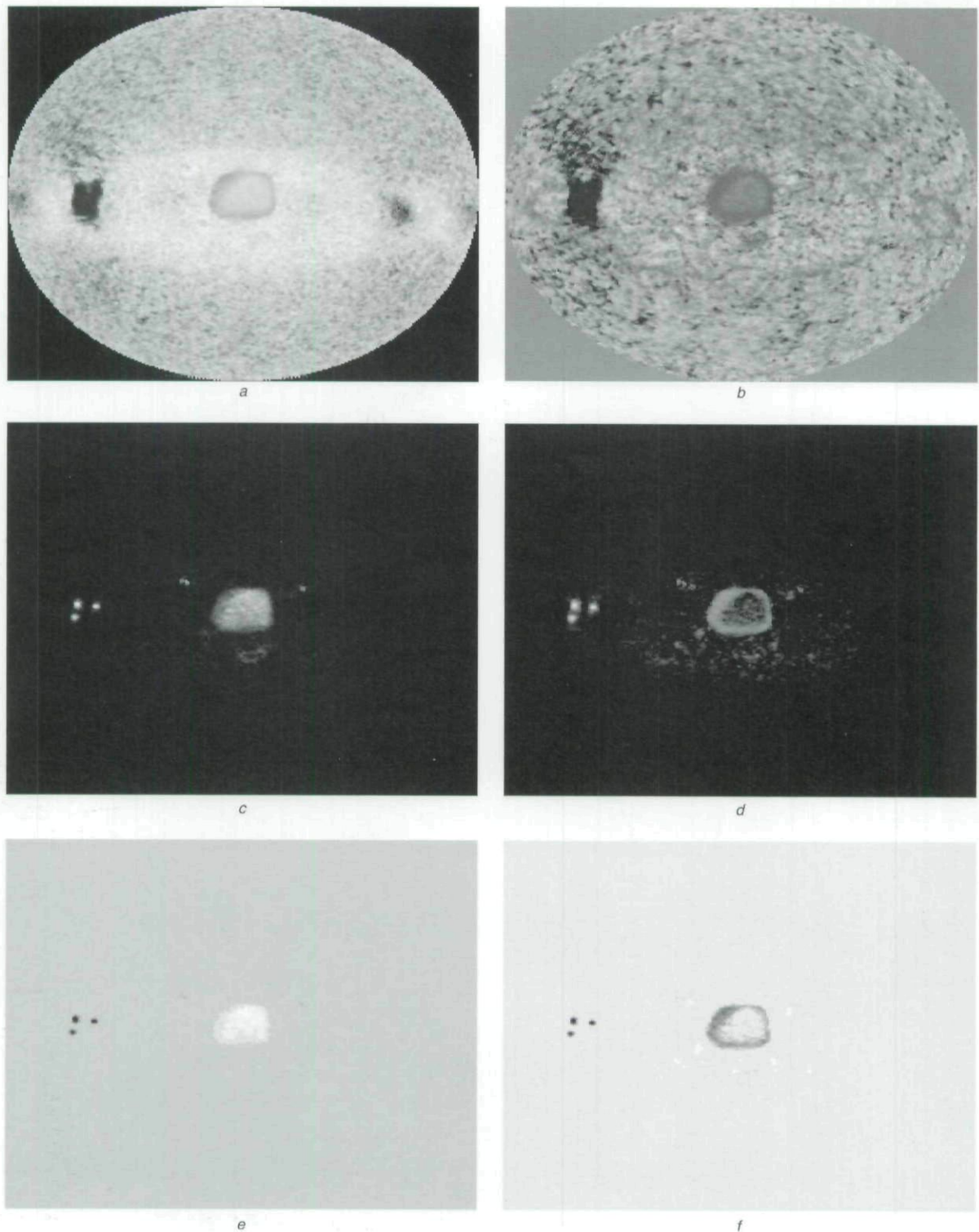
Fig. 3 *Similarity maps of dynamic PET study shown in Fig. 1 calculated using reference ROI placed over normal tissue and similarity measures (a) COR, (b) NCOR, (c) SSQ, (d) SQS, (e) SC and (f) CS*

Table 2 Contrast values for ROI_b and ROI_m for dynamic PET study

ROI	COR	NCOR	SSQ	SQS	SC	CS
ROI_b	0.18	0.69	23.0	18.0	0.0	54.0
ROI_m	0.0	0.34	0.0	0.0	0.0	0.0

4 Discussion

This study focused on exploring the role of similarity mapping in oncological dynamic PET studies and addressing the problem of enhanced localisation of lesions and metastases.

SM segments regions in the dynamic images according to their temporal rather than their spatial properties. It has been applied to dynamic MRI data sets and has successfully identified various structures such as the renal cortex and medulla (ROGOWSKA *et al.*, 1995), low grade astrocytoma (ROGOWSKA *et al.*, 1994), activated areas of the brain during photic stimulation (ROGOWSKA *et al.*, 1995) and activated areas of the motor-cortex during finger motion (BANDETTINI *et al.*, 1993), ischaemia in the left coronary artery territory and focal ischaemia in the brain (ROGOWSKA *et al.*, 1995), breast tumours (LUCAS-QUESADA *et al.*, 1996), lung tumour and tentorial meningioma (ROGOWSKA *et al.*, 1995).
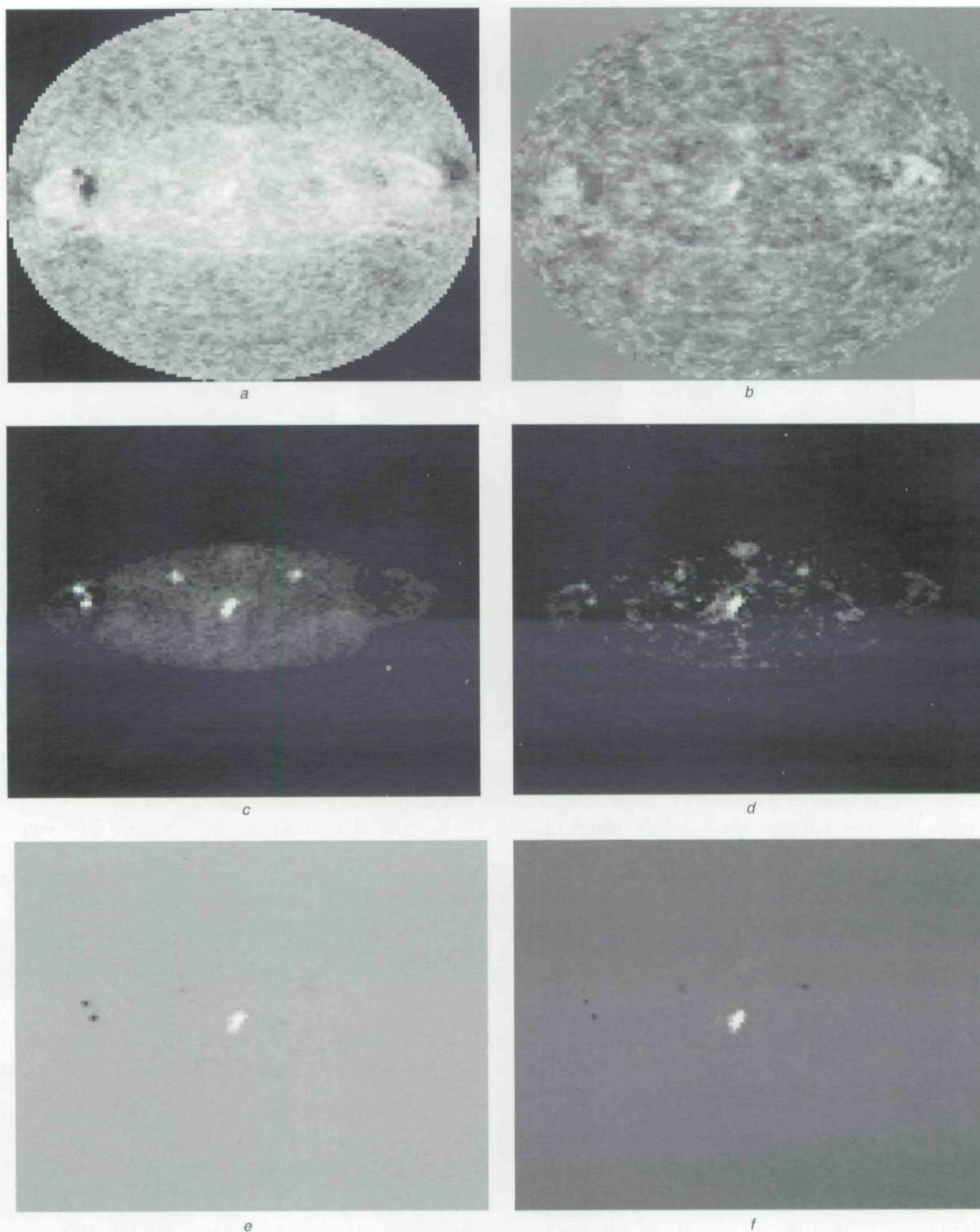
Fig. 4 *Similarity maps of clinical data set of colorectal recurrence calculated using tumour reference VOI and similarity measures (a) COR, (b) NCOR, (c) SSQ, (d) SQS, (e) SC and (f) CS*

We have used two previously described formulas for the calculation of similarity maps, COR and NCOR, and we have introduced four new similarity measures: SSQ, SQS, SC and CS. Use of the correlation-based similarity metrics has been selected as the most commonly used methodology for

Table 3   Contrast values for clinical patient study

COR	NCOR	SSQ	SQS	SC	CS
0.0	0.0	3.55	30.9	0.35	2.45

Table 4   Detectability of clinically significant tissues and organs in similarity map images of clinical data studies. Numbers represent fraction of cases

	Tumour	Vessels
COR	no (20/20)	no (20/20)
NCOR	no (20/20)	no (20/20)
SSQ	yes (20/20)	yes (20/20)
SQS	yes (20/20)	slightly (18/20)
SC	yes (17/20)	negatively (20/20)
CS	yes (20/20)	negatively (20/20)
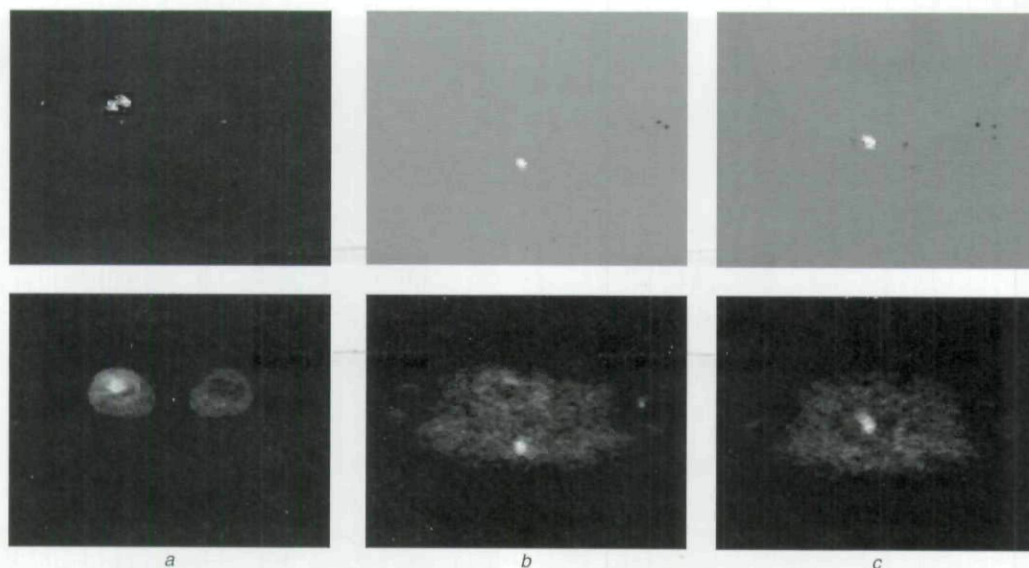
Fig. 5 *Similarity CS maps (upper row) and SUV images (lower row) from three transaxial slices from dynamic PET studies of patients with giant cell tumour of right tibia (left column) and recurrent colorectal tumour (middle and right columns)*

comparison of the similarity between images or image segments. The use of these metrics stems from the fact that the Euclidean distance D between two image vectors x and y or image segments can describe a measure of the dissimilarity between these two: $D^2 = \sum_i [x(i) - y(i)]^2$. It can be shown that the correlation measure $\sum_i x(i)y(i)$ is included as one of the factors of the expansion of the Euclidean distance: $D^2 = \sum_i [x(i)]^2 - 2_i[x(i)]^2 \sum 2_i x(i)y(i) + \sum_i [y(i)]^2$. The use of the normalised version of the correlation measure is dictated by the need to provide a metric independent of parameters such as changes in the count rates, differences in the study and the camera parameters and other additive or multiplicative factors that could appear in images acquired at different times.

In this study, the COR and NCOR maps could discriminate between structures in the dynamic phantom data set, whereas they were ineffective in separating structures in clinical data. Higher background noise, lower resolution and less structural information in dynamic PET images compared with dynamic MRI scans could account for the different performance of those similarity measures. Unlike COR and NCOR, the new measures managed to reveal the structures of interest. Particularly, CS provided better parametric images and would be the method of choice as far as discrimination between the tumour and other structures was concerned, both on simulated phantom studies and clinical data from PET studies of colorectal tumour recurrences (even in the vicinity of hot organs such as the bladder) and giant cell tumour. Structures are instantly identified in the similarity maps, as vessels are either absent (when the bladder is present) or displayed is different scales of grey.

The selection of the reference ROI depends on the clinical question being asked and provides different kinds of information. Using a reference ROI placed over the bladder could reveal a small lesion in its vicinity obscured by its higher activity in the original image set. Even though an ROI placed

over the normal tissue can also delineate the tumour in a simple phantom study, for clinical data sets, this was shown to be inefficient. In cases where a tumour is clearly visible in the original image, an ROI placed over it could help detect small metastases, under the condition that these have the same metabolic rate and behaviour in time as the tumour selected. Partial volume effects can be an additional source of error; however, as SM images show enhanced contrast for areas of interest, it is expected that the detection of small lesions would also be improved.

As manual selection of the reference ROI could be time consuming and prone to operator bias, research is ongoing into the development of a semi-automatic technique for the optimum selection of a reference ROI by the testing of many possible reference pixels using a maximum entropy method (ROGOWSKA and WOLF, 1992). At the same time, this operator bias affects the sensitivity and specificity of the technique, as the manual selection of the reference ROI could also affect the probability of reaching false-negative or false-positive diagnoses. This is expected to be improved when a semi-automatic or fully automatic ROI selection method is introduced.

We have shown that SM and SUV images have comparable diagnostic performance, although SM is able to offer additional, time-related information in a single image. SM images summarise the underlying kinetics of the radiotracer uptake, whereas SUV offers information only on the static image frame (here, at 55–60 min post-injection) under evaluation, independent of the previous image frames. Similarity maps could therefore be an alternative, offering specific advantages, to SUV-based evaluation for studies that require dynamic PET acquisitions.

In fact, the use of SUV as a method of classification of tissue areas as benign or malignant is still under discussion among nuclear medicine physicians and oncologists (KEYES, 1995; HUANG, 2000), as high metabolic activity (reflected by FDG uptake) can arise for a large number of reasons that are not related to tumours. A wide variety of benign disorders have high SUVs (LAPELA *et al.*, 2000) including inflammation areas, a common cause of 'false positive' ^{18}F-FDG PET scans (STRAUSS, 1996). On the other hand, some malignant lesions may not necessarily have particularly high SUVs. Furthermore, high degrees of fluctuation for the SUVs from one day to another have been observed.

Table 5   Contrast values for CS and SUV images for two types of tumour

	CS	SUV
Colorectal recurrences	2.36 ± 0.47	4.12 ± 0.42
Giant cell tumour	11.6 ± 2.1	11.9 ± 1.8

Camera quality controls and calibrations are other parameters on which SUV measurements depend. In addition, there is currently no proper study on the dependence of SUVs on the type of PET camera used (i.e. BGO against LSO-based tomographs etc.), or on the data processing prior to image formation, such as attenuation and scatter correction, efficiency normalisation methods etc., and some studies have already indicated dependence on the image reconstruction method (VISVIKIS *et al.*, 2001). Therefore the utility of the information provided by the SUVs largely depends on its integration with all the available clinical and instrumental data (LUCIGNANI *et al.*, 2004).

SM could facilitate visual evaluation, by summarising the information about the temporal dynamics of structures in one image and improving the detectability of tumours and metastases, especially in cases where poor image quality, due to lack of iterative image reconstruction or lesion characteristics (size, location etc.), complicates the visual interpretation of dynamic ^{18}F-FDG-PET data sets. On the other hand, given the dynamic process that represents the FGD uptake in tissue, dynamic ^{18}F-FDG-PET is the most appropriate procedure for oncological studies. However, the fact that such explorations are, in general, time-consuming (although efficient alternatives to solve this problem have been recently presented (STRAUSS *et al.*, 2003)) and more expensive has prohibited, until now, the spread of this powerful technique in routine oncological PET explorations. It would be interesting also to explore the performance of the newly introduced similarity measures in other fields of dynamic PET imaging as well as in dynamic MRI scans.

5 Conclusions

Although similarity mapping has successfully identified various structures in dynamic MRI data sets, its potential application to dynamic PET data sets has not yet been sufficiently studied. In this work, a feasibility study of the use of similarity maps in the extraction of features with diagnostic and general clinical interest from dynamic PET images has been presented. The goal of the present study was not to present a tool of clinical utility, but to offer a method for nuclear medicine physicians to proceed to further detailed clinical evaluation and validation studies of the proposed technique.

Similarity mapping could be a more appropriate diagnostic technique than the SUV approach, especially in dynamic PET. It has been also argued that dynamic PET is a more appropriate acquisition protocol for oncological studies for cancer diagnosis and therapy management than conventional, static, whole-body acquisitions.

The present study showed that the newly introduced CS similarity map criterion rapidly identifies structures with similar temporal properties, has comparable contrast to SUV images and could enhance the detection of tumours that might not be easily discriminated in the original images. Therefore similarity mapping based on this measure could successfully be used to support the visual interpretation of dynamic ^{18}F-FDG PET data sets in oncology. The performance of the newly introduced similarity measures in other fields of dynamic PET imaging, as well as in dynamic MRI scans, is under study.

References

ADAM, L. E., ZAERS, J., OSTERTAG, J. H., TROJAN, H., BELLEMANN, M. E., and BRIX, G. (1997): 'Performance evaluation of the whole-body PET scanner ECAT EXACT HR/sup +/following the IEC standard', *IEEE Trans. Nucl. Sci.*, **44**, pp. 1172–1179

ALAVI, A., and REIVICH, M. (2002): 'Guest editorial: the conception of FDG-PET imaging', *Semin. Nucl. Med.*, **32**, pp. 2–5

AMARAL, T. G., CRISOSTOMO, M. M., and DE ALMEIDA, A. T. (1998): 'Fuzzy segmentation-an important tool in image processing'. *Proc. IEEE World Congress on Computational Intelligence*, **2**, pp. 1577–1582

BANDETTINI, P. A., JESMANOWICZ, A., WONG, E. C., and HYDE, J. S. (1993): 'Processing strategies for time-course data sets in functional MRI of the human brain', *MRM*, **30**, pp. 161–173

BARNEA, D. I., and SILVERMAN, H. F. (1972): 'A class of algorithms for the fast digital image registration', *IEEE Trans. Comput.*, **21**, pp. 179–186

BOUDRAA, A.-O., CHAMPIER, J., DJEBALI, M., BEHLOUL, F., and BEGHDADI, A. (1999): 'Analysis of dynamic nuclear cardiac images by covariance function', *Comput. Med. Imag. Graph.*, **23**, pp. 181–191

BOUDRAA, A.-O., BEHLOUL, F., JANIER, M., CANET, E., CHAMPIER, J., ROUX, J.-P., and REVEL, D. (2001): 'Temporal covariance analysis of 1rst-pass contrast-enhanced myocardial magnetic resonance images', *Comput. Biol. Med.*, **31**, pp. 133–142

BRIX, G., ZAERS, J., ADAM, L. E., BELLEMANN, M. E., OSTERTAG, H., TROJAN, H., HABERKORN, U., DOLL, J., OBERDORFER, F., and LORENZ, W. J. (1997): 'Performance evaluation of a whole-body PET scanner using the NEMA protocol', *J. Nucl. Med.*, **38**, pp. 1614–1623

CONNINE, C. M., TITONE, D., DEELMAN, T., and BLASKO, D. (1997): 'Similarity mapping in spoken word recognition', *J. Memory Lang.*, **37**, pp. 463–480

DUFOURNAUD, Y., SCHMID, C., and HORAUD, R. (2004): 'Image matching with scale adjustment', *Comput. Vis. Image Und.*, **93**, pp. 175–194

GAMBHIR, S. S., CZERNIN, J., SCHWIMMER, J., SILVERMAN, D. H. S., COLEMAN, E., and PHELPS, M. E. (2001): 'A tabulated summary of the FDG PET literatura', *J. Nucl. Med.*, **42**, pp. 1S–93S

HUANG, S.-C. (2000): 'Anatomy of SUV', *Nucl. Med. Biol.*, **27**, pp. 643–646

HYMAN, T., ROTHMANN, C., HELLER, A., MALIK, Z., and SALZBERG, S. (2001): 'Structural characterization of erythroid and megakaryocytic differentiation in Friend erythroleukemia cells', *Exper. Hematol.*, **29**, pp. 563–571

JERUSALEM, G., HUSTINX, R., BEGUIN, Y., and FILLET, G. (2003): 'PET scan imaging in oncology', *Eur. J. Cancer*, **39**, pp. 1525–1534

KEYES, J. W. (1995): 'SUV: standard uptake or silly useless value?', *J. Nucl. Med.*, **36**, pp. 1836–1839

KONTAXAKIS, G., STRAUSS, L. G., THIREOU, T., LEDESMA-CARBAYO, M. J., SANTOS, A., PAVLOPOULOS, S., and DIMITRAKOPOULOU-STRAUSS, A. (2002): 'Iterative image reconstruction for clinical PET using ordered subsets, median root prior and a Web-based interface', *Mol. Imag. Biol.*, **4**, pp. 219–231

LAPELA, M., EIGTVED, A., JYRKKI, S., *et al.*, (2000): 'Experience in qualitative and quantitative FDG PET in follow-up of patients with suspected recurrence from head and neck cancer', *Eur. J. Cancer*, **36**, pp. 858–867

LEE, J. S., LEE, D. D., CHOI, S., PARK, K. S., and LEE, D. S. (2001): 'Non-negative matrix factorization of dynamic images in nuclear medicine', *IEEE Nuclear Science Symposium Conference Record*, **4**, pp. 2027–2030

LO, E. H., ROGOWSKA, J., BOGORODZKI, P., TROCHA, M., MATSUMOTO, K., SAFFRAN, B., and WOLF, G. L. (1996): 'Temporal correlation analysis of penumbral dynamics in focal cerebral ischemia', *J. Cereb. Blood Flow Metab.*, **16**, pp. 60–68

LUCAS-QUESADA, F. A., SINHA, U., and SINHA, S. (1996): 'Segmentation strategies for breast tumors from dynamic MR images', *JMRI*, **6**, pp. 753–763

LUCIGNANI, G., PAGANELLI, G., and BOMBARDIERI, E. (2004): 'The use of standardized uptake values for assessing FDG uptake with PET in oncology: a clinical perspective', *Nucl. Med. Commun.*, **25**, pp. 651–656

PHELPS, M. E. (2004): 'PET—molecular imaging and its biological applications' (Springer Science and Business Media, NY, 2004)

ROGOWSKA, J., and WOLF, G. L. (1992): 'Temporal correlation images derived from sequential MR scans', *J. Comput. Assist. Tomogr.*, **16**, pp. 784–788

ROGOWSKA, J., PRESTON Jr, K., ARONEN, H. J., and WOLF, G. L. (1994): 'A comparative analysis of similarity mapping and eigen-imaging as applied to dynamic MR imaging of low grade astro-cytoma', *Acta Radiologica*, **35**, pp. 371–377

ROGOWSKA, J., PRESTON, K., HUNTER, G. J., HAMBERG, L. M., KWONG, K. K., SALONEN, O., and WOLF, G. L. (1995): 'Applications of similarity mapping in dynamic MRI', *IEEE Trans. Med. Imag.*, **14**, pp. 480–486

ROTHMANN, C., LEVINSHAL, T., TIMAN, B., AVTALION, R. R., and MALIK, Z. (2000): 'Spectral imaging of red blood cells in experimental anemia of Cyprinus carpio', *Compar. Biochem. Physiol. A*, **125**, pp. 75–83

STRAUSS, L. G., and CONTI, P. S. (1991): 'The applications of PET in clinical oncology', *J. Nucl. Med.*, **32**, pp. 623–648

STRAUSS, L. G. (1996): 'F-18 deoxyglucose and false-positive results: a major problem in the diagnostics of oncological patients', *Eur. J. Nucl. Med.*, **23**, pp. 1409–1415

STRAUSS, L. G., KONTAXAKIS, G., DIMITRAKOPOULOU-STRAUSS, A., PAVLOPOULOS, S., and SANTOS LLEO, A. (1998): 'Parametric imaging of dynamic PET studies, based on compartmental and non-compartmental approaches', *Eur. J. Nucl. Med.*, **25**, p. 938

STRAUSS, L. G., DIMITRAKOPOULOU-STRAUSS, A., and HABERKORN, U. (2003): 'Shortened PET data acquisition protocol for the quantification of ^{18}F-FDG kinetics', *J. Nucl. Med.*, **44**, pp. 1933–1939

TANIMOTO, T. T. (1961): 'A nonlinear model for a computer-assisted medical diagnostic procedure', *New York Acad. Sci. Trans. (ser. II)*, **23**, pp. 576–578

THIREOU, T., STRAUSS, L. G., DIMITRAKOPOULOU-STRAUSS, A., KONTAXAKIS, G., PAVLOPOULOS, S., and SANTOS, A. (2003): 'Performance evaluation of principal component analysis in dynamic FDG-PET studies of recurrent colorectal cancer', *Comput. Med. Imaging Graphics*, **27**, pp. 43–51

TOORONGIAN, S. A., MULHOLLAND, G. K., JEWETT, D. M., BACHELOR, M. A., and KILBOURN, M. R. (1990): 'Routine production of 2-deoxy-2(F-18)fluoro-D-glucose by direct nucleophilic exchange on a quaternary 4-amino-pyridinium resin', *Nucl. Med. Biol.*, **3**, pp. 273–279

VENOT, A., LEBRUCHEC, J. F., and ROUCAYROL, J. C. (1984): 'A new class of similarity measures for robust image registration', *Comput. Vis. Graphics Image Proc.*, **28**, pp. 176–184

VISVIKIS, D., CHEZE-LeREST, C., COSTA, D. C., BOMANJI, J., GACINOVIC, S., and ELL, P. J. (2001): 'Influence of OSEM and segmented attenuation correction in the calculation of standardised uptake values for [18F]FDG PET', *Eur. J. Nucl. Med.*, **28**, pp. 1326–1335

Author's biography

TRIAS THIREOU holds a diploma in Physics and the MS degree in Bioinformatics from the University of Athens, Greece and the MS and PhD degrees in Biomedical Engineering, joined from the National Technical University of Athens and the School of Medicine, University of Patras, Greece. She is currently a postdoctoral fellow at the Institute of Computer Science of the Foundation for Research and Technology – Hellas (ICS-FORTH). Her main research interests include medical image reconstruction and analysis, Monte Carlo simulations, machine learning methods and computational biology.